

# PACS – Realization of an adaptive concept using pressure actuated cellular structures

B. Gramüller, J. Boblenz, C. Hühne

German Aerospace Center, Institute of Composite Structures and Adaptive Systems

E-Mail: [benjamin.gramueller@dlr.de](mailto:benjamin.gramueller@dlr.de)

## Abstract

A biologically inspired concept is investigated which can be utilized to develop energy efficient, lightweight and applicational flexible adaptive structures. Building a real life morphing unit is an ambitious task as the numerous works in the particular field show. Summarizing fundamental demands and barriers regarding shape changing structures, the basic challenges of designing morphing structures are listed. The concept of Pressure Actuated Cellular Structures (PACS) is arranged within the recent morphing activities and it is shown that it complies with the underlying demands. Systematically divided into energy-related and structural subcomponents the working principle is illuminated and relationships between basic design parameters are expressed. The analytical background describing the physical mechanisms of PACS is presented in concentrated manner. This work focuses on the procedure of dimensioning, realizing and experimental testing of a single cell and a single row cantilever made of PACS. The experimental outcomes as well as the results from the FEM computations are used for evaluating the analytical methods. The functionality of the basic principle is thus validated and open issues are determined pointing the way ahead.

## 1 Introduction

Fluidic actuators can be used to integrally combine an efficient, lightweight and accurate drive system with a deformable structure. The advantages of pneumatic and hydraulic actuators compared with other drive systems are examined by Huber (Huber J. E. et al., 1997). The specific stresses and strains as well as the resolution of motion of this actuators lead to a wide range of use and predestinates it for aeronautical applications. In nature, the combination of fluidic actuation and shape variable structure can be discovered at a special group of plants. Representatives like the thigmonastic Cape Sundew (*Drosera Capensis*) and Venus Flytrap (*Dionaea Muscipula*), which use their touch sensing capabilities to trap small insects are examples for a successful implementation of biological integral morphing structures. Another common example is given by the seismonastic Mimosa Pudica that protects its fragile leafage through a folding mechanism when shaken. Sibaoka, investigated the mechanisms of nastic plants. He describes the loss and gain of turgor - internal hydrostatic cell sap pressure - (symbolized by  $H_2O$  in at the lower left depiction of Figure 1) as the driving force for the distortions (Sibaoka, 1991), which leads to cell pressures of more than 8MPa (Howard, 1991).

Researchers working on form variable structures made huge efforts to adapt this principle to a mechanically usable structural system. The technology of pressure driven adaptive cell and in particular honeycomb structures is investigated by M. Barrett and R. Vos. Filed in 2010 they hold the patent for the method and apparatus for pressure adaptive morphing structure (Barrett R. et al., 2010) (Vos R. et al., 2010). Vos et al. developed a pressurized honeycomb concept for actuating their Pressure Adaptive Gurney Flap. This trailing edge flap autonomously changes its shape in different flight altitudes and takes advantage of aerostatic pressure differences (Vos R. et al., Pressure Adaptive Honeycomb: Mechanics, Modeling, and Experimental Investigation, 2010). Recently two very similar concepts followed this idea, a topology-optimized design for morphing airfoils (Vasista S. et al., 2013) and an adaptive pressure-controlled compliant structure for linear motion (Luo Q. et al., 2013). The work on pressurized cellular structures is an ongoing endeavor.

Pagitz et al. transferred the idea of fluidic pressure driven morphing structures into a two dimensional concept with a promising degree of deformation, high flexibility and sizeable characteristic (Pagitz M. et al., 2012) and patented (Pagitz M. et al., 2011). They showed with analytical methods how the deformational shape of such a structure can be controlled for

multiple cells and cell rows making certain assumptions for the mechanics of flexure hinges (Pagitz M. et al., Compliant Pressure Actuated Cellular Structures, 2014). The form-finding approach they established allows conceiving structures to vary their shapes stepless between multiple form functions. The concept of pressure actuated cellular structures (PACS) can be seen as initial point for this research. Figure 1 summarizes the preceding work on shape changing structures using pressurized cellular structures.

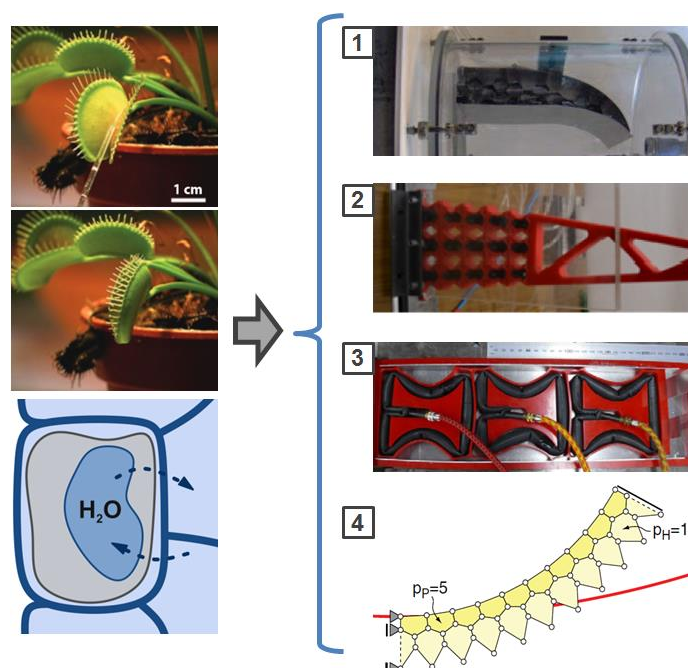
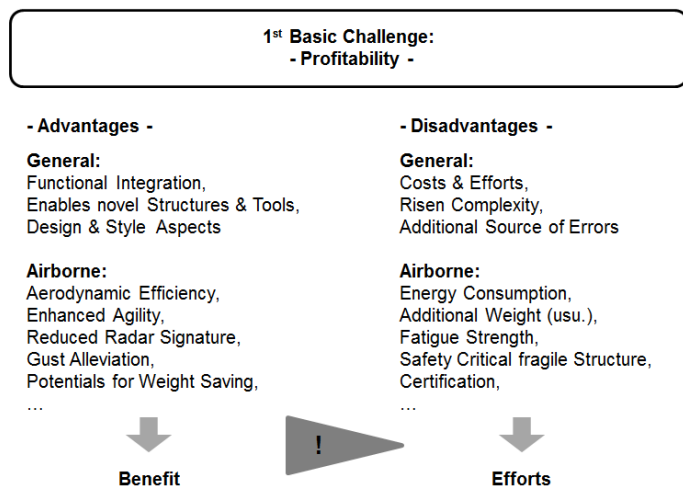


Figure 1: Example from nature: Venus Flytrap (*Dionaea Muscipula*; left); Concepts of deduced operating principle: (1) Pressure Adaptive Gurney Flap (Vos R. et al., Pressure Adaptive Honeycomb: Mechanics, Modeling, and Experimental Investigation, 2010), (2) topology optimized design from Vasista (Vasista S. et al., 2013), (3) compliant structure for linear motion (Luo Q. et al., 2013) and (4) PACS (Pagitz M. et al., 2012)

## 2 Demands on Adaptive Structures and Difficulties

The design of conventional structures is usually driven by two groups of requirements. The first one is of programmatic manner and holds general demands like low costs, high quality and reduced development time. As a second group, structural demands with reference to structural mechanics are determined by the expected loads and in addition by geometrical requirements. As these needs are also valid for shape variable structures a PACS has to withstand the design loads and simultaneously ensure to keep deformations in a tolerable range. In the case of PACS the actuator can be divided in two functional elements, the energy adjusting element (e.g. compressor), which transforms energy (e.g. electrical energy) from the auxiliary energy source into a usable energy form (e.g. pressure and volume) and the energy converter, that modifies the received energy in order to obtain the desired energy driven effects (e.g. deformation) (Janocha, 1992). Each of these elements and their sub-elements own a particular efficiency coefficient which has to be as high as possible and affects the overall power demand of the active structure. Together with the increased complexity the power demands and the additional weight of the energy converter, adjusting element and peripheral sub components like wiring, the first basic problem about shape variable active structures appears. It can be condensed to the following: "The development and implementation of a concept for shape changing structures is only reasonable if the anticipated benefit outweighs the invested efforts." Figure 2 specifies this general demand.



**Figure 2: Challenge of generating profitable adaptive structures**

The energy consumption and related peripheral weight, depends on the required forces and travel ranges needed to deform the structure. Common concepts for aeronautical shape variable structures like the horn concept (Mueller, 2000), the ripless plain flap (Bauer, 2000), the active flexspar actuator (Barrett R. et al., Missile flight control using active, 1996) and the vertebrate structure (Elzey D. et al., 2003) are in need of stiff and weighty structural components to withstand aerodynamic forces. On the contrary Barrett et al. even describe the possibility of reducing structural weight by adaptive structures. An artificial muscle structure, based on the pressure driven honeycomb, benefits of its weight efficient structural integrated actuator and provides the non-concentrated forwarding of distributed aerodynamic loads. Structural hard points can thus be eliminated for further weight reduction and provide an additional contribution to the advantages for airborne applications (Barrett R. et al., Biomimetic FAA-certifiable, artificial muscle structures for commercial aircraft wings, 2014).

A raise of structural stiffness increases the sufferable external forces on the corresponding structure but heightens the necessary efforts for changing the structures shape and limits the boundaries of tolerable deformation. Thus the second challenge of developing a profitable morphing concept can be formulated: "An efficient concept for shape variable structures circumvents the seeming contradiction of a specific design being stiff and flexible at the same time." (see Figure 3) There are some concepts available which have implemented this principle, like the flexible rib from Monner (Monner, 2001), the cellular planar morphing structure from Vasista (Vasista S. et al., 2013), the tendon-actuated compliant cellular trusses (Ramrakhyani D. et al., 2005) or the zigzag wingbox (Ajaj R.M. et al., 2012). The common principle behind these examples is a steered release of specific degrees of freedom (dofs) by integrating hinges, compliant mechanisms or linear bearings.

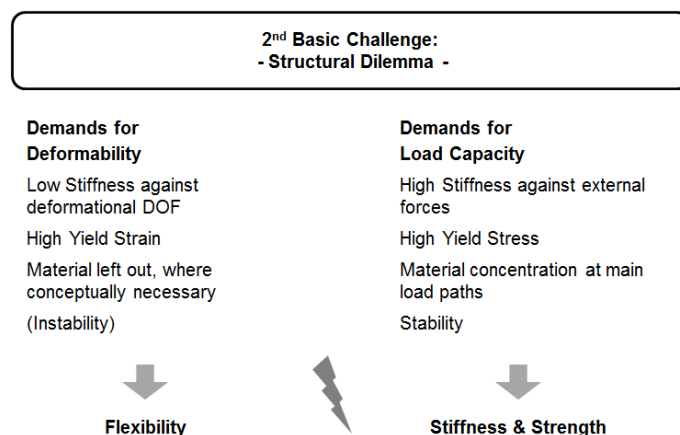


**Figure 3: Morphing concepts and structural dilemma**

Other demands on the morphing structure's actuation element concern its performance-based properties, the maximum forces respectively momentums, e.g. stall torque for an electric motor, and the related travel ranges. Regarding the combination of actuator and structure, the structural response, depending on the actuators characteristics as well as on the structural stiffness and mass distribution, underlies the requirements for control speed and frequency and is essential for the definition of the operating range of such a concept. Other, not unique airborne subjects as fatigue strength and certification are essential for building a real life morphing structure. Before investigating efforts in these topics, the potentials of a concept for adaptive structures are revealed in this further step of doing research into PACS.

Pressure actuated honeycomb structures and PACS share most of their advantages and disadvantages. Their potential for future airborne or general structures is based on its lightweight and energetically efficient actuation and design. The different concepts about using the cell interior pressurization to cause deformations on an exterior surface result in the need of a separated consideration of this concept. PACS are conceptualized to generate two-dimensional deformations on single-curved surfaces. The conceivable operating range regarding structural dimensions can be varied from centimeters to meters without having any losses of functionality, due to the possibility of adapting certain counteracting design variables. This concept is characterized by a blended structure-actuator construction, possesses a necessary minimum of stiffness in the hinge regions of the cells and generates structural stiffness through pressurization. The individual shape of each PACS cell allows defining the local deformations during changes in pressure. High flexibility in shape variations and applicability result for this structure.

### 3 Physics of PACS

#### 3.1 Background

The functional principle of pressure actuated cellular structures is based on the increase of entropy  $\Delta S$  due to the reduction of inner energy  $\Delta U$  by volume maximization  $V$ . Equation two describes the relation between the enthalpy  $\Delta H$ , the inner energy and the ideal gas equation with its amount of substance  $n$ , ideal gas constant  $R$  and temperature  $T$ . The inner energy is calculated with the system's pressure  $p$ , the ambient pressure  $p_a$  and the system's volume  $V$  (see equation 3). Figure 4-1 provides a comprehensible visualization of the effects, which lead to the driving forces of this concept. Similar to a flattened balloon, a flexible membrane does not have any defined state of shape without being pressurized. Not until the membrane is loaded with a particular inner pressure  $p$  the resulting distribution of forces lead onto bending moments. As long as  $p$  exceeds the ambient pressure  $p_\infty$  these bending moments can cause deformations. Through the extension of the fluid the pressure is minimized ( $p_1 > p_2 > p_3$ ) and equally the inner energy is reduced.

$$\Delta S = -\frac{\Delta H}{T} \quad (1)$$

$$\Delta H = \Delta U + \frac{\Delta nRT}{const} \quad (2)$$

$$\Delta U = -\int_1^2 \frac{(p(V) - p_a)}{const} \partial V = (p - p_a)(V_1 - V_2) \quad (3)$$

Adapted to the cellular structure with the assumptions of rigid cell sides and infinitesimal stiff hinges, shown at the second depiction, the inner volume of this five-edged single cell can only be enlarged by varying the angle between neighbored cell sides. The equilibrium state is equally reached when the trapped volume is maximized. Due to the conceptual idea the pressure stays constant during the deformation process. Assuming infinite bending flexibility, a structural shape of maximum volume is reached for a cell pressure  $p_1$  that exceeds the ambient pressure  $p_\infty$  by at least an infinitesimal value ( $p_1 - p_\infty > 0$ ).

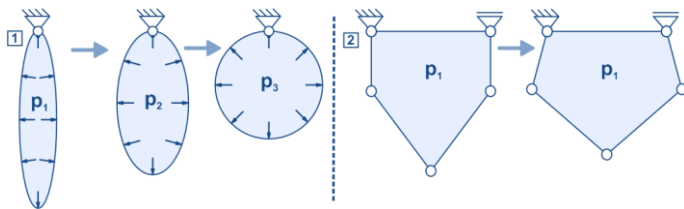


Figure 4: Schematic diagram of (1) adiabatic expansion of pressurized fluid within flexible membrane (2) isobaric increase in volume within pressured cell

#### 3.2 Mechanical model of compliant PACS

Each single cell in the basic idea of compliant PACS consists of two structural elements, faces and hinges. The face element is assumed to hold infinite stiffness. In a two-dimensional consideration it can be modeled as rigid body element by two nodes with two translational dofs each, namely  $u_x$  and  $u_y$ . Pressure induced distributed loads result in normal forces  $N_j$  and shear forces  $Q_j$  at cell side  $j$  with length  $a_j$  as well as in bending moments  $M_k$  at hinge  $k$ . Cell side elements are connected among themselves by one-dimensional compliant hinge elements. Regarding the deformation behavior of PACS, the main difference between a flexible hinge joint and a compliant hinge is stated in its non-zero bending stiffness.

Compared to that of cell side elements it is assumed to be very low and can be substituted by rotational springs. The one node element thus holds the additional dof  $r_z$  and possesses a hinge geometry dependent stiffness constant  $c_k$ . For a compliant hinge with the constant wall thickness  $t_k$  the hinge length  $s_k$  and a uniform bending moment  $M_k^c$  the compensatory spring stiffness is calculated to

$$c_k = \frac{M_k^c}{\Delta \alpha_k} = E \frac{I_{z,k}}{s_k} = E \frac{t_k^3}{12s_k} \quad (4)$$

Providing the required energy for the actuation of the structure the encapsulated fluid initiates forces on the wetted face regions. This pressure induced loading leads to the initial force and moment distribution shown in Figure 5.

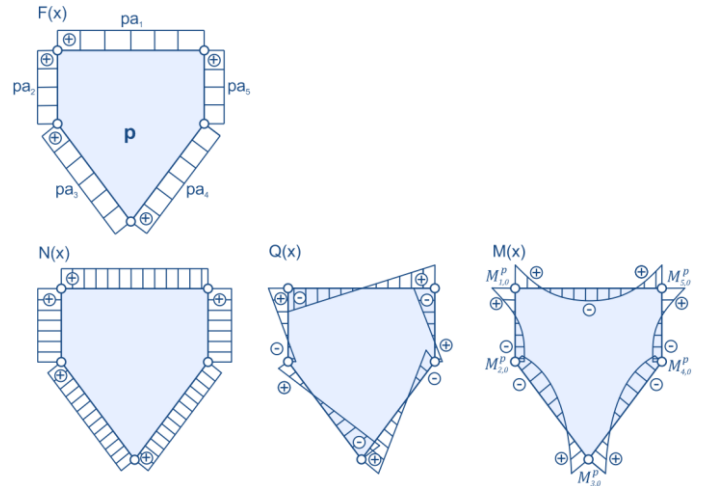


Figure 5: Initial pressure load, normal, shear force and momentum distribution on five edged cell

The equilibrium state of the structure is reached when the sum of pressure induced moments  $M_k^p$  and hinge stiffness induced moments  $M_k^c$  vanishes.

$$M_k^c + M_k^p = 0 \quad (5)$$

Because of the geometrical highly nonlinear behavior of this system, the pressure induced momentums depend on the current state of deformation. Although a direct calculation of the equilibrium state is possible for a single cell, for a multi-cell structure an iterative numerical approach is recommended. As this paper focuses on the procedure of dimensioning, realizing and testing, the computational background of designing PACS consisting of a huge number of cells has to be obtained from the underlying works (Pagitz M. et al., 2012).

#### 3.3 Design parameters

The starting point of designing PACS for a real life application is given by the outcomes of the computational investigations that are not part of this paper, as stated in 3.2. Resulting in a two dimensional truss structure these calculations preliminarily define the parameters:

- 1) Initial cell geometry and size
- 2) Maximum pressure
- 3) Maximum rotation at hinges
- 4) Forces and momentums

Two parameters are determined additionally within the process of generating a three dimensional structure complying with the computed information:



- 5) Wall and hinge geometry
- 6) Material

The geometry of the cell sides and the hinges together with the characteristics of the chosen material have to be determined to withstand the loads on the structure which are prescribed by the parameters 1-4. As the hinge geometry has huge influence on its stiffness properties, the functionality of the PACS has to be preserved moreover. For the following calculations an axial cell length of one is assumed.

### 3.3.1 Cell sides

The cell sides, assumed to own infinite stiffness, are the first elements to size. Stresses from normal forces and bending momentums have to be considered during the wall thickness calculations. Therefore the following specific values can be obtained from the preliminary calculations:  $a_j, p, N_j, M_k$ . The normal forces are constant over the face length and can be written as

$$N_j(x) = N_j = \text{const} \quad \begin{array}{c} \leftarrow N_j \quad \quad \quad N_j \rightarrow \\ \text{---} \end{array} \quad (6)$$

The related tangential stresses of a cell side of thickness  $t_j$  at length  $x$  result in

$$\sigma_{j,Nt}(x) = \frac{N_j}{t_j(x)} \quad (7)$$

Bending moments are responsible for both tangential stresses and cell side deflection. In order to reduce the bending of cell walls which separate areas of different fluidic pressure and to calculate the bending induced stresses the function for the local bending moments  $M_j(x)$  is calculated. The underlying shear forces are

$$Q_{j,1} = -Q_{j,2} = -\frac{M_k + M_{k+1}}{a_j} \quad \begin{array}{c} M_k \quad \quad \quad pa_j \quad \quad \quad M_{k+1} \\ \downarrow \quad \quad \quad \uparrow \quad \quad \quad \downarrow \\ \text{---} \\ \uparrow \quad \quad \quad \downarrow \\ 0.5pa_j + Q_{j,1} \quad \quad \quad 0.5pa_j + Q_{j,2} \end{array} \quad (8)$$

$$Q_j(x) = px + \left( \frac{M_k + M_{k+1}}{a_j} - \frac{pa_j}{2} \right) \quad (9)$$

The shear forces  $Q_{j,1}$  and  $Q_{j,2}$  result from the equilibrium of moments at hinge  $k$  and  $k+1$ . The appropriate bending moment is calculated as the integral of shear force over  $x$

$$M_j(x) = \frac{1}{2}px^2 + \left( \frac{M_k + M_{k+1}}{a_j} - \frac{pa_j}{2} \right)x + M_k \quad (10)$$

The maximum tangential stress due to bending at the extreme fiber (tensile stress) is with equation (4) calculated to

$$\sigma_{j,Mt} \left( x, y = \frac{t_j(x)}{2} \right) = \frac{|M_j(x)|}{I_j(x)} \frac{t_j(x)}{2} = 6 \frac{|M_j(x)|}{t_j^2(x)} \quad (11)$$

The tangential stresses from normal forces and bending moments overlay at the extreme fiber. The maximum stresses at the cell sides can be written as

$$\sigma_{j,tot} = 6 \frac{|M_j(x)|}{t_j^2(x)} + \frac{N_j}{t_j(x)} \quad (12)$$

The minimum wall thickness leading to a reliable PACS at the location of maximum bending moment and thus maximum tangential stress is calculated as

$$t_{j,min} = \frac{N_j + \sqrt{N_j^2 + 24R|M_j(x)|_{max}}}{2R} \quad (13)$$

for the cell sides.  $R$  is the yield stress of the applied material.

### 3.3.2 Compliant hinges

The definition of the geometry for the compliant hinges is also done analytically. The following equations were formulated on basis of two assumptions. The maximum stresses appear at the maximum pressure. This assumption has to be considered in the predesign. Its validity depends on the overall stiffness and the amount of pressure applied to PACS. Further the momentum at each hinge is assumed to be constant over its length  $s_k$ . The validity of this proposition strongly depends on the load transfer of tangential forces and thus the hinge orientation and geometry.

The tangential force at an arbitrary hinge is calculated using the pipe formula. It can be used in regions where the cell reaches the stiffening phase (see chapter 3.5). At this state of shape, all edges approximately lay on a circular arc.

$$N_k = pr \quad (14)$$

The momentum  $M_k$  can be extracted from the preliminary computations. The maximum stresses at the extreme fiber of the compliant hinge is

$$\sigma_{k,tot} = \sigma_{k,M} + \sigma_{k,N} = \frac{6|M_k|}{t_k^2} + \frac{pr}{t_k} \quad (15)$$

For the hinge geometry the minimum wall thickness results in

$$t_{k,min} = \frac{pr + \sqrt{(pr)^2 + 24R|M_k|}}{2R} \quad (16)$$

### 3.4 Coupling of design parameters

The hinge geometry determines the bending stiffness of the joints and thus the flexibility of the whole structure. It influences the equilibrium state of the pressurized structure and thus couples with the force and momentum parameters initially taken as an input for this design step. An iterative process would solve this problem by adapting the hinge geometry according to the current PACS until the parameters are in equilibrium. There are two coupling effects:

- The equilibrium state of structure depends on the hinge stiffness and
- the hinge momentums are relative to the state variable  $\Delta\alpha_k$

Remedy can be provided by directly calculating the hinge momentum from the angular distortion.

$$M_k = \frac{Et_k^3}{12s_k} \Delta\alpha_k \quad (17)$$

The hinge thickness is essential for both the strength of the PACS and for its flexibility and influences the momentum  $M_k$ . The possibility of increasing the strength of a specific hinge is

limited through the fact that the momentum raises with this thickness for a given angular distortion. This approach opens the possibility to find an optimum value which yields the thickness that allows applying the maximum pressure on a given PACS cell. The maximum stress  $\sigma_k$  for the distortion  $\Delta\alpha_k$  and a material with stiffness  $E$  is

$$\sigma_{k,tot} = E \frac{|\Delta\alpha_k| t_k}{s_k} + \frac{pr}{t_k} \quad (18)$$

The optimum hinge thickness is calculated with

$$p(t) = \left( R - E \frac{|\Delta\alpha_k| t_k}{s_k} \right) \frac{t_k}{r} \quad (19)$$

$$\frac{\partial p(t)}{\partial t} = \left( R - E \frac{|\Delta\alpha_k| t_k}{s_k} \right) \frac{1}{r} \stackrel{t_k=t_{k,opt}}{=} 0 \quad (20)$$

to

$$t_{k,opt} = \frac{R s_k}{E |\Delta\alpha_k|} \quad (21)$$

Inserting this formula into equation (19) results in

$$p_{k,max} = \frac{1}{2} \frac{R^2 s_k}{E r |\Delta\alpha_k|} \quad (22)$$

For receiving a constant value for the maximum pressure for all hinges and equally pressured cell rows, the quotient  $s_k/|\Delta\alpha_k|$  should be constant. In order to find the optimum material for a given PACS, the maximum for this equation has to be computed. Figure 6 shows the results of investigating five material groups, fiber reinforced polymers (FRP) from in-house material characterizations, elastomers (Wacker, 2014), metals (Böge, 2007), plastics (Hornbogen, 2006) (Kern, 2014) and ceramics (Weißbach W., 2007) for their potential to deliver the maximum pressure value. The material of each group which leads to the highest pressure value determines the boundary of pressurization for a given hinge distortion  $\Delta\alpha_k$ . The cell's radius is 25mm and the hinge lengths are unified to  $0.1r$  for this depiction. As the hinges are the most critical elements of the structure, this graph shows the limits of mechanical resilience of PACS and forms the design envelope for a single cell for reasonable hinge distortions  $0.5^\circ \dots 15^\circ$ .

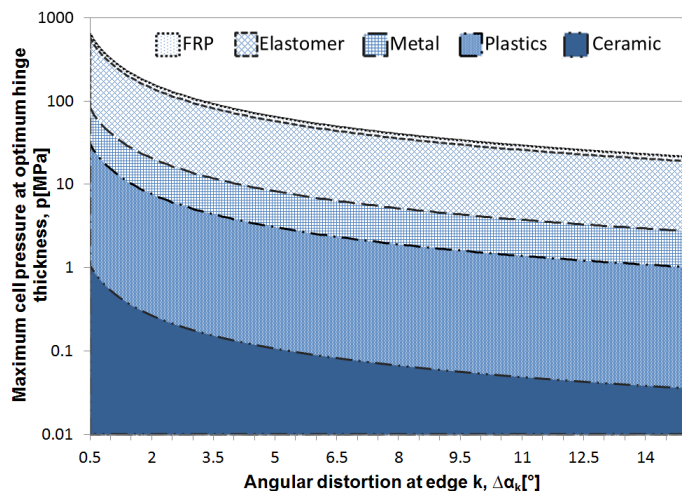


Figure 6: Design envelope for a cell of  $r=25\text{mm}$  and  $s_k=0.2r$

FRP materials with the highest  $R^2/E$  ratio deliver the best performance for the given boundary conditions (see equ.22). For the unidirectional CFRP (Carbon FRP) T800+M21 which builds the upper boundary of the graph, the characteristic values in fiber direction and the affected limit values for  $\Delta\alpha_k = 15^\circ$  are given in Table 1. It holds the calculational results for static loads and material constants not adapted for fatigue requirements. Sun Z. et al. investigated composite mechanics and pose that static load and appropriate material characteristics can only provide limited results. As stated in their work, for a fatigue designing of FRP structures the number of load cycles within a full component life of estimated  $1e5$  load cycles lead to a significant reduction of material strength. For a  $90^\circ$  CFRP laminate layup a strength loss of about 30% was measured (Sun Z. et al., 2003). In the further investigations, the characteristic strength values of suitable materials have to be reduced for fatigue conditions. In this work static values are used in order to show the functionality of the concept and to compare static design values with static experimental loads. The methodology of sizing PACS structures is generic and can be fitted to individual stress limits as well as to other boundary conditions.

Table 1: T800+M21 and resulting thickness and maximum pressure

Material	Young's Modulus [GPa]	Max Stress [MPa]	$t_{opt}$ [mm]	$p_{max}$ [MPa]
T800+M21 [0] <sub>s</sub>	161	3011	0.36	21.5

The iteration process for finding the equilibrium state of PACS during the adaption of the hinge geometry cannot be avoided. The impact of changing the stiffness parameter  $c_k$  is depicted in Figure 7. The structural parameters used for generating this graph are extracted from the demonstrator design and presented in chapter 4.

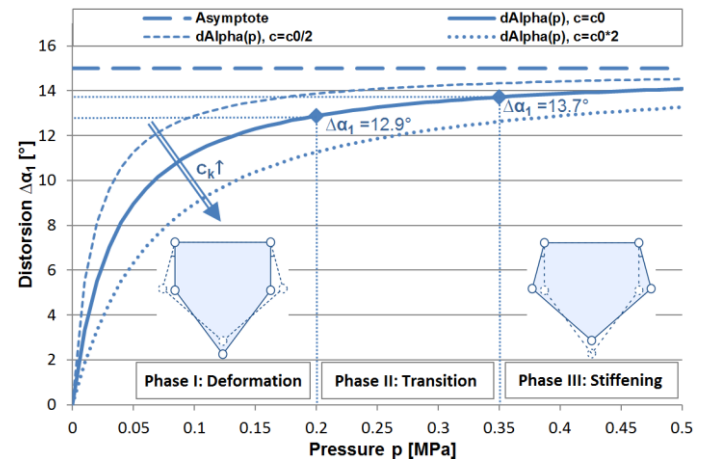


Figure 7: Pressure dependent deformation  $\Delta\alpha_1$  of a single cell, with a width of 50mm and an asymptotic distortion of  $15^\circ$

The effects of modifying the stiffness matrix  $c$  for the hinges of a single cell are substantial for the pressure dependent pathway of distortion. The division of this behavior in its three phases is made in the following.

### 3.5 Pressure induced deformation behavior

The cell geometry outlined in Figure 9 shows the pressure dependent deformation given in Figure 7. The state function  $\alpha_1(p)$  holds an asymptotic pathway between zero deformation at zero pressure and its defined limit value of  $\Delta\alpha_1 = 15^\circ$  for an infinite amount of pressure. The behavior between can be divided into three phases. Within the "Deformation Phase" the cell distorts from the unstressed manufacturing shape into a geometrical state of about  $90^\circ$

percent of deformation to the asymptotic value. This phase is responsible for the deformation of the PACS yet it does not provide the required stiffness towards external forces. The "Transition Phase" represents the conjunction between phase I and III, where minor distortions still occur and the stiffening of the cell is already initiated. In phase III the deformation of the structure is minimal. A rise of pressure only leads to an increase of stiffness.

This behavior is also valid for multi cell structures. For the single row cantilever characterized in this paper, it is true that the higher the pressure the stiffer the PACS.

## 4 Design Process

A single row cantilever is designed with the dimensions  $300 \times 50 \times 450 \text{mm}^3$  consisting of six pentagonal cells. The analytical predesign is followed by the material section and the definition of the geometry for hinges and cell sides. The subsequent numerical examination of the resulting structure shall verify the previous outcomes.

### 4.1 Preliminary computations

The target structure is designed to perform an angular distortion of  $30^\circ$  per cell for infinitesimal hinge stiffness ( $c \rightarrow 0$ ). The rotation of the last surface cell side is thus  $(6 - 2 * 0.5) * 30^\circ = 150^\circ$ . This large deformation per cell was chosen in order to demonstrate the potential of PACS.

Figure 8 shows the equilibrium state of the compliant PACS structure at  $p=0.35 \text{MPa}$ . The geometry and material input for the underlying calculations are defined within this chapter. In addition the PACS cantilever is shown loaded with a horizontal force of  $F_x = 100 \text{N}$  to give a feeling for its stiffness.

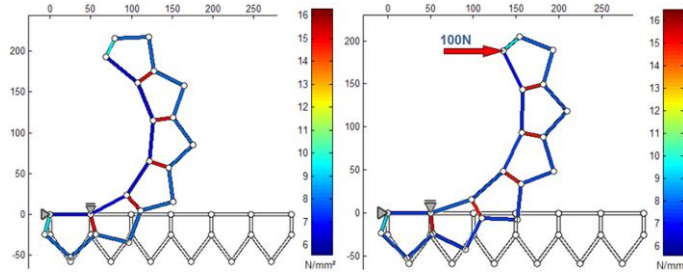


Figure 8: Equilibrium state and normal stresses of single row cantilever demonstrator without and with external loads

The normal forces and momentums respectively hinge distortions of this PACS are used together with the equations from chapter 3 for the following sizing process.

### 4.2 Cell dimensioning

The results from the preliminary calculations are used to choose a suitable material and to create a detailed three dimensional geometry for the PACS.

#### 4.2.1 Material selection

The preceding investigations showed that the hinge areas are the critical elements of a PACS to size. Besides the priorly formulated mechanical requirements on the hinge region two other demands appear. The optimum wall thickness which is analytically determined may be limited by manufacturing conditions. Depending on the sort of material the geometry and manufacturing process specific thickness limitations exist. Additionally for finite pressure values it may be recommendable to reduce the hinge thickness in order to reach the stiffening phase and converge with the asymptotic distortion (see Figure

7). The material which is used to accomplish a real life demonstrator furthermore has to own a high strength to stiffness ratio (see equation 22).

For the target structures, the single cell and the single row cantilever, the best results are attained with uni-directional (UD) fiber reinforced plastics. UD-FRP appeared to be the most efficient material for these boundary conditions from mechanical point of view and coincidentally allows realizing wall thicknesses below  $0.5 \text{mm}$ . The GFRP (glass FRP) material HexPly913 is chosen for this demonstrator because of its suitable ply thickness and processability. Using HexPly913 the integrity of the structure at the test conditions could be ensured. The results are presented the following. Table 2 shows the respective material constants.

Table 2: Material data for GFRP HexPly913, (type NVE 913/28%/192/EC9756)

$E_{  } [\text{GPa}]$	$E_{\perp} [\text{GPa}]$	$R_{  } [\text{MPa}]$	$R_{\perp} [\text{MPa}]$	$\nu [-]$	$t_{\text{ply}} [\text{mm}]$
42.00	14.50	1194.30	197.65	0.29	0.125

#### 4.2.2 Stress calculation

The introduced equations for finding a reliable design for PACS are used to confirm the manually defined GFRP layout. The notation, geometry and laminate layup for the symmetrical cell is shown in Figure 9. The outer hinge radius is identical for all of the five positions and determined to  $r_o = 3 \text{mm}$ .

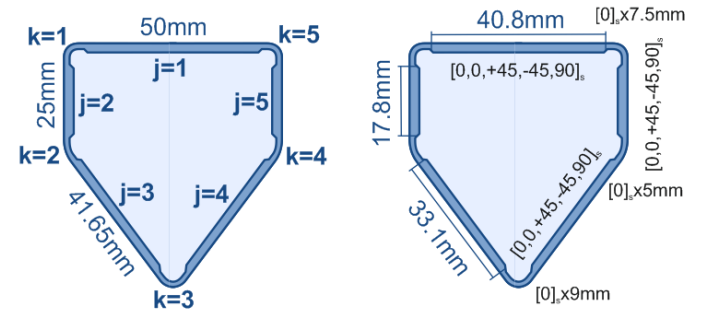


Figure 9: Notation, geometry and laminate layup for the single cell demonstrator

The two enwrapping plies are orientated in circumferential direction in order to take advantage of the huge stiffness and strength characteristics in fiber direction. Increased bending stiffness at the face areas as well as high load capacity for the compliant hinges result from this design.

For a maximum pressure of  $0.35 \text{MPa}$ , the depicted laminate layup with a ply thickness of  $0.125 \text{mm}$ , the following values are calculated for the symmetric single cell

Table 3: Results from analytical calculations

Position		1	2	3
Cell Sides	$N_{j,max} [\text{N}]$	6.98	10.18	8.37
	$M_{j,max} [\text{Nm}]$	107.58	28.98	77.16
	$\sigma_{j,tot} [\text{MPa}]$	287.36	68.03	195.72
Hinges	$c_k [\text{Nm}]$	7.29	10.94	6.08
	$M_k [\text{Nm}]$	1.79	-4.86	2.41
	$\sigma_{k,tot} [\text{MPa}]$	207.01	501.55	266.71
	$\Delta\alpha_k [^\circ]$	14.08	-25.46	22.76

The single cell can be compared with the most highly loaded cell of the single row cantilever. As the first and sixth cell also possess an uncoupled cell side at  $j = 2$  respectively  $j = 5$ , the maximum loading of these cells can thus be reproduced. The related laminate properties in circumferential direction are

**Table 4: Laminate properties**

Position	Lam. Stiffness II [GPa]	Lam. Strength II [MPa]	Wall Thickness [mm]
Cell Sides	35.79	521.49	1.25
Hinges	42.00	1194.30	0.25

The evaluation of the analytically computed stress values lead to a safety factor of  $SF_{an,H} = 2.38$  for the hinge elements and  $SF_{an,CS} = 1.81$  for the cell sides. The FEM based simulation shall verify these results.

**4.3 Numerical simulation**

Using MSC Patran for pre- and postprocessing and MSC Nastran for the task of solving the FEM model, numerical simulations are performed. The supplementary numerical calculation yields an additional value for the design because it holds the detailed geometrical information about the elements hinge and cell side. The assumptions made for the analytical design - constant moments over hinge length and maximum pressure delivers maximum stresses - can be dropped. Also the geometrical nonlinear behavior of the cell elements can be simulated. A resolution of 5.3e3 elements for the single cell and 19.6e3 elements for the cantilever were carefully chosen after investigating the total deformation over element size. A doubling of element quantity leads to a deviation of maximum strain below 1.7% at the extreme fiber. Shell elements provide accuracy and save solving time compared to three dimensional elements. For thin walled structures like these the use of 2D elements is valid.

Hinge lines are considered as discrete one-dimensional components possessing a specific geometry dependent bending stiffness within the analytical approach. For the numerical calculation a geometrical model is built which includes the real geometry of the compliant hinge. Both the effective hinge position due to this geometry and the deformation of the hinge und face elements during pressurization are considered. The stress and strain distribution as well as the overall deformation at the individual FRP laminae can be examined.

By applying the maximum pressure of 0.35MPa in an arbitrary number of load steps, the results can be observed during deformation.

The detailed geometry information for the preliminary designed cell and the respective laminate setup can be taken from Figure 9. For the cantilever demonstrator the design has to be adapted in order to ensure functionality. The compliant hinges at the intersection points of the neighbored cell sides  $j = 5$  and  $j = 2$  have to be shifted to an eccentric position as it is shown in Figure 10.

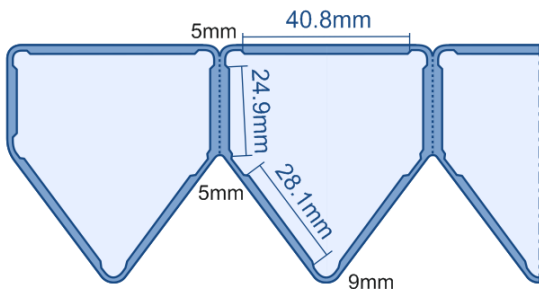


**Figure 10: Adapted cell geometry for demonstrator application**

Both, the single cell and the cantilever are simulated to be compared with the previous work steps.

Figure 11 shows the undeformed and deformed mesh of the numerical model as well as the related stress distribution at the comparative pressure of 0.35MPa. The results are posed for the outmost ply, at middle, in circumferential direction.

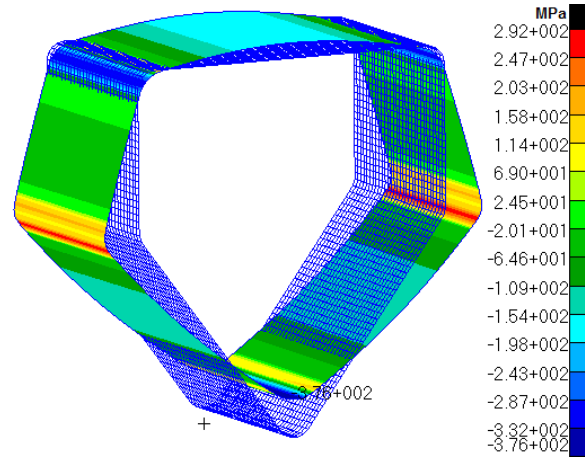


**Figure 11: Maximum ply (at middle) stress results of outer laminae for p=0.35MPa in circumferential direction from FEM simulation - Single Cell**

The most important value for the comparison of the results from the two types of computation is the distortion of hinge 1. It is equal to  $\Delta\alpha_5$  and responsible for the deformation of the upper surface of the cantilever.

**Table 5: Comparison of deformation results for single cell**

$\Delta\alpha_{1,an.} [^\circ]$	$\Delta\alpha_{1,FEM} [^\circ]$	$\eta_{an,FEM} [\%]$
14.08	13.01	+8.22

Reasons for the variance of analytical and numerical results can be found in the local stress distribution at the hinge regions. The non-uniform and locally concentrated distortions and stresses lead to increased hinge stiffness. Together with the information about the effects of hinge stiffening explained in Figure 7 this result is suitable with the expectations. A detailed comparison and failure analysis, for the analytical method, the numerical investigations and experimental data is presented within chapter 6.

The six cell PACS with its adjusted cell geometry is simulated equally. Figure 12 delivers the maximum ply stress distribution for a position at the middle of the plies and the associated deformations.

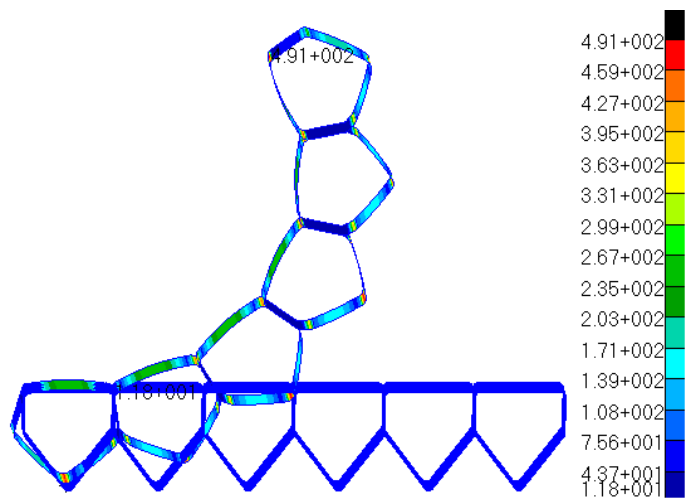


**Figure 12: Maximum ply (at middle) stress results for p=0.35MPa in circumferential direction from FEM simulation - single row cantilever**

Equally to the single cell, the FEM results show a reduced deformation. The geometrical modifications intensify the deviation per cell. The following table shows the angle of the surface cell side ( $j=1$ ) at the sixth cell for analytical and FEM computations.



**Table 6: Comparison of deformation results for the single row cantilever at cell side one of cell six at  $p = 0.35MPa$**

$\Delta\beta_{6,1,an.} [^\circ]$	$\Delta\beta_{6,1,FEM} [^\circ]$	$\eta_{an.,FEM} [\%]$
140.79	113.88	+23.63

The examination of stresses outputs a maximum value of  $\sigma_{x,max,FEM} = 920.61MPa$  and a minimum of  $\sigma_{x,max,FEM} = -843.27MPa$  at the hinge elements extreme fiber in circumferential direction. The maximum absolute stress value for cell side elements lays a factor four below the hinge values and are not critical. At  $p = 0.35MPa$  a safety factor of  $SF_{FEM,H} = 1.30$  results. The evaluation of the concept in the form of a physical demonstrator can be processed on the basis of these investigations.

## 5 Prototype

A single cell and a single row cantilever are built. For the cantilever demonstrator six cells of width 50mm and length 450mm are used to reach an entire span of 300mm. All of the cells are designed to have the same dimensions in order to simplify manufacturing. The ability to prove the concept for its practicability and evaluate the calculation results is thus not reduced. The possibilities to uncover material dependent manufacturing issues and to develop suitable concepts for applying a certain amount of pressure onto the cells are further reasons for this demonstrator.

### 5.1 Manufacturing

After defining the cell's geometry and local wall thicknesses, a mold is designed in order to produce a suitable core where the GFRP material can be wound upon. Geometrical adaptations considering thermal expansion during the autoclave process are necessary. The single cell is manufactured using a silicone core from the two component elastomer Wacker Elastosil 4642. This silicone core leads to a smooth inner surface and can be demolded from the GFRP structure easily and non-destructive.

Preforming the inner face plies increases accuracy and facilitates draping. The manufacturing process was optimized for the single cell before starting with the cantilever. The parameters of the autoclave process for curing this prepreg material are given in Figure 14. The autoclave process influences the quality of the manufacturing results, in particular, for the single row cantilever. The first phase of the autoclave process, where the setup is heated up to  $T_A = 80^\circ C$  reduces the viscosity of the uncured resin and initiates the curing process. The autoclave pressure of  $p_A = 0.6MPa$  is applied to the evacuated specimen for compacting the structure and rises the fiber volume fraction.

Insufficient tautness of the hinge plies frequently resulted in wrinkles at the sensible compliant hinge regions and could not be eradicated by increased drape efforts. In addition to the curing process, the temperature value controls the thermal expansion of the GFRP material and of the silicone core. The effects of expansion shall on the one hand be limited to ensure dimensional accuracy and on the other hand are used to stretch and straighten the circumferential fibers by enlarging the cells perimeter to avoid wrinkles (cf. Figure 13).

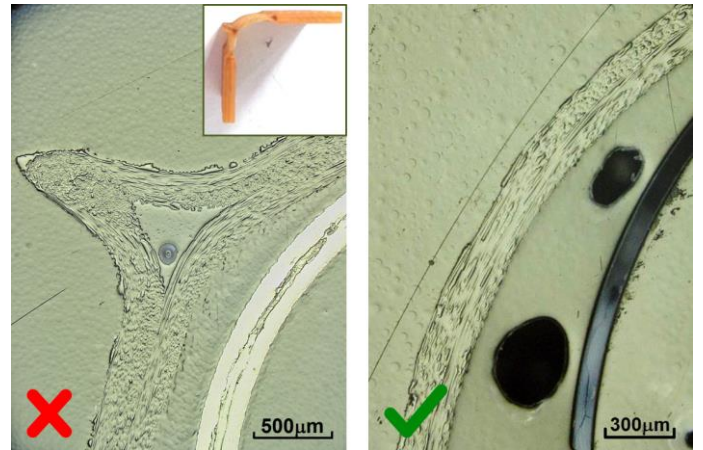


**Figure 13: Cell hinge at position 1 with and without wrinkles**

The curing strategy depicted in Figure 14 was experimentally optimized to provide a solution for this problem. At the end of phase 1, the chemical reactions are most widely completed. The second phase subsequently is responsible for completing reactions of the residual uncured resin at  $T_A = 130^\circ C$ .

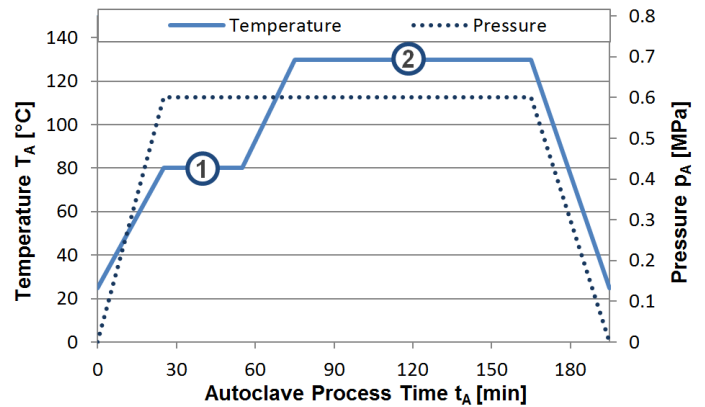


**Figure 14: Autoclave curing process for single cell and single row cantilever processing**

The most critical regions for the manufacturing process are located where three cell sides join together. The final solution for the eccentric compliant hinges is shown in Figure 15. The upper crossing point is realized by simply coupling the inmost and outmost plies. The intermediate resin reservoir builds a very small gusset of 1mm in diameter. A second possibility was implemented for a better support of the intersection's geometry. The depiction at the bottom shows a comparatively huge crossing area, with a diameter of 4mm. The stiffening appeared to be necessary due to the autoclave process and the differential pressure of 7MPa forcing the cells to drift away from each other. A stable geometry for this gusset could not be implemented without the additional material accumulation.



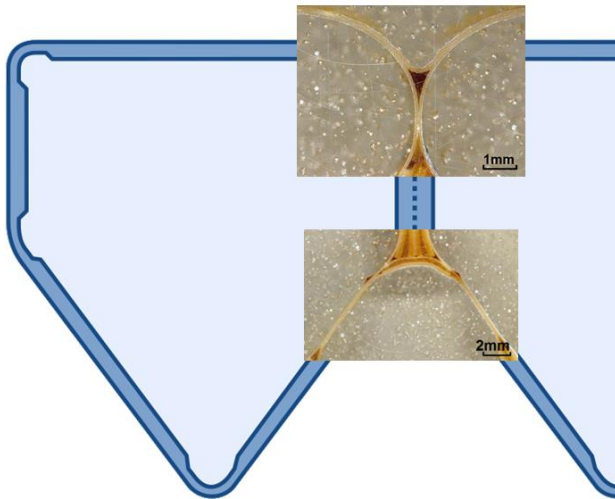


**Figure 15: Eccentric compliant hinges at crossing points of adjacent cells**

Some of the specimens used for preliminary investigations referring to the cantilever are depicted in Figure 16. The microscope photographs are taken for quality management and show a typical hinge face transition of the single cell at the top right depiction. The preformed face package and the enshrining 0° plies can be perceived.

Possible hinge geometries at the crossover sections of neighbored cell sides were tested for functionality and manufacturability. Figure 16 shows multiple two cell production trials on the left, and in the downright depiction a microscopic image of the successful implementation of this compliant hinge joint for fiber composite structures. As it can be seen, the enveloping plies with circumferential fiber direction enclose the preformed face laminate and forms a smooth resin braced transition between faces and hinges.

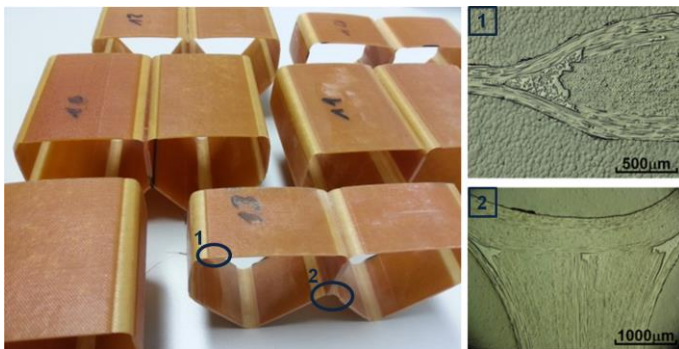


**Figure 16: Manufacturing approaches and appropriate microscope photographs**

The single row cantilever prototype could be built completely integrally with the described process.

## 5.2 Pressurization

A basic issue about the idea of PACS is the implementation of a reliable concept for pressurizing the cells. For the mentioned prototypes, a pressurization system is developed which allows charging the structure with a pressure of 0.35MPa. At this point the stiffening phase is reached and the cells' deformation is most widely finished.

The requirements on such a system prevent to use a solution off the shelf. A new development is inevitable. Figure 17 summarizes the most influential requirements for the conceiving process.

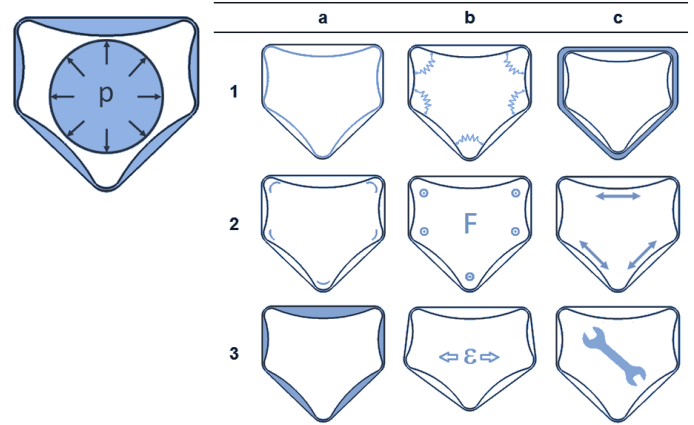


**Figure 17: Visualization of the three groups a, b, c of functional requirements for pressurization concepts**

Within the first column three criteria are listed concerning the quality of pressurizing the surface. These requirements demand...

- a1 the charge of the inner faces with a constant pressure distribution,
- a2 the pressurization of also the hinge areas, and
- a3 a minimized or infinitesimal edge region at both of the cells' ends, where the pressure distribution differs from the constant value.

Furthermore the fluid sealing structure is to be constructed to have certain mechanical characteristics. They arise from material properties combined with geometrical design and are composed of...

- b1 an infinitesimal resistance against deformation or a supportive mode of action to foster hinge distortion,
- b2 the structural strength to withstand forces from pressurization and
- b3 the overall flexibility necessary to tolerate the applied deformation.

The third group of requirements affects the boundary conditions arising from a multi cell structure. In an accumulation of numerous cells...

- c1 the geometrical space around the cells contour is limited by neighbored cells or other surrounding structure,
- c2 a variety of different cell sizes and geometries exist, which should be encapsulated with one and the same universal concept, and
- c3 in case of failure or maintenance the system has to be renewable.

According to this list of requirements, three suitable concepts are found, which overtop others in consequence of their particular advantages referring to one or more of these demands.

The advantages of the first concept concern the groups (a) and (c) of the requirements. Adhesively casting the cells' open face with an elastomeric material leads to a completely pressurizable inner cell surface, complies with geometrical boundaries and is adaptive to arbitrary cell geometries (see Figure 18-1). FEM based simulations are processed and show a tolerable stiffness against hinge distortion at values up to  $\Delta\alpha = 10^\circ$  per functional face.

A further high potential concept is designed to make use of the enclosed pressured fluid in the same way the respective cell does. Figure 18-2 shows the geometry that supports the cell's deformation for a positive  $\Delta\alpha_1$  and  $\Delta\alpha_5$ . The basic idea of generating the DSEC's (Deformation Supportive End Cap)

shape is to balance the needed strain energy at deformation with the potential energy provided by the fluid.

Computing an isotenoid end cap for the asymptotic state of a cell builds the starting point of the geometry generation. This cap does not bring distortional forces to the cell structure for any pressures at the asymptotic state. Deformed in deviant state shape it pursues to reach the previous condition in the same way, the cellular structure does.

Further, two possibilities can be chosen to process this functionality. The simple variant is to manufacture the end cap in the asymptotic geometry. It can be assembled with the cell by manually deforming the cell to this state.

The more complex approach adapts the cap's geometry in the way that the resulting pressure dependent forces compensate those, resulting from the cap's deformation and material stiffness. Hereby the cap can be mounted to the undeformed cell structure without being distorted during joining. This principle also works for positive and negative distortions. In general there are two possible implementations of this concept, the already mentioned isotenoid multi-curved solution, which is shown below, and a compliant version with flexure hinges and rigid faces. Both of the types will fulfill the requirements of group (a) and (b), but are underprivileged regarding variable cell geometries and maintenance. The DSEC shall provide the possibility to combine an energetically efficient self-induced deforming mechanism with a high level of material utilization. The processing of such caps and the examination of the respective stiffness properties is part of the subsequent work. The endeavor of generating a PACS structure that outperforms common non-adaptive structures in terms of lightweight and structural efficiency is in need of an end cap solution that saves these advantages. A lightweight cellular structure with a heavy pressurization concept is not expedient.

The third concept accomplishes all of the underlying requirements with slight disadvantages towards constant pressure distribution, fluid transfer and adaptability of cell geometries. A flexible tube of elastomeric material together with rigid load carrying end caps which minimize the effective cross section at the cell's open ends is shown in Figure 18-3. It represents an efficient exchangeable cartridge system with external fluid feeding, suitable for pressures up to 0.35MPa for the given prototype geometry. The self-sealing fluid-tight conic press fit, coincidentally building the rigid end cap is shown in a pulled out position. A centric tension rod, for carrying axial loads, connects both of the opposite caps, mount them against each other and brace the tube material at pressurization. This concept was selected to be used for the following work as it is easy to assemble and proved itself in practice for the necessary test pressures.

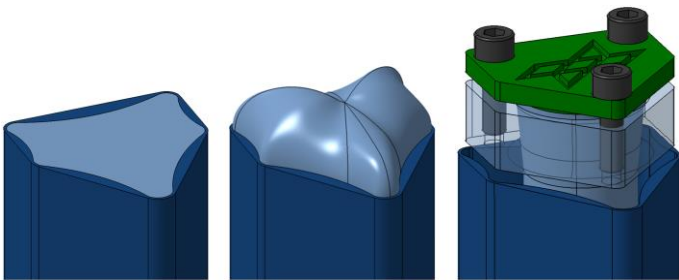


Figure 18: End cap concepts: (1) Shape Adaptive Cell Cast, (2) DSEC - Deformation Supportive End Cap, (3) Tube Cartridge

### 5.3 Demonstrators and test arrangement

The first demonstrator, the Single Cell, is used to investigate the mechanical behavior of the PACS during pressurization. A digital barometer for quantifying the pressure within the tube cartridge and a laser-supported distance meter provide the

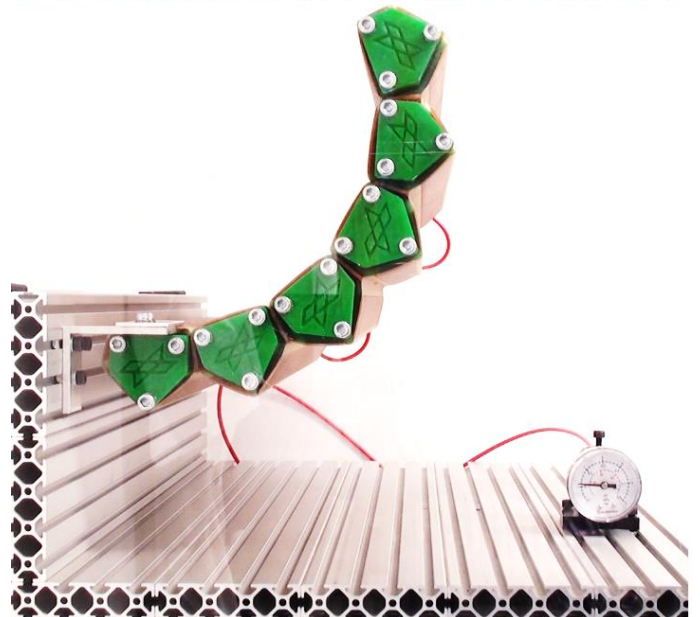
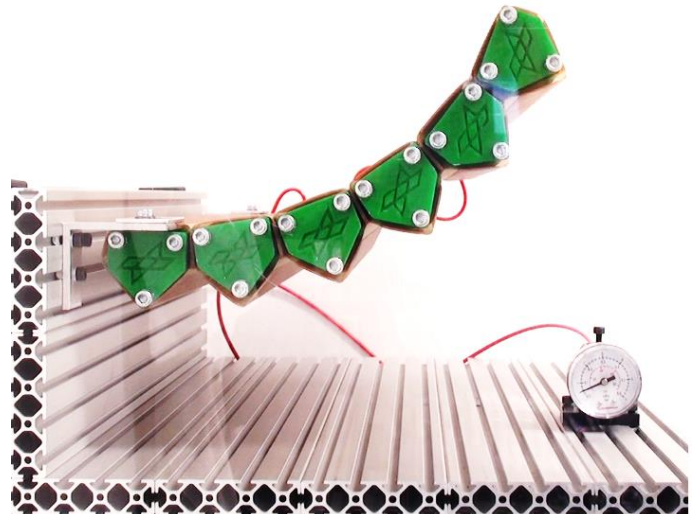
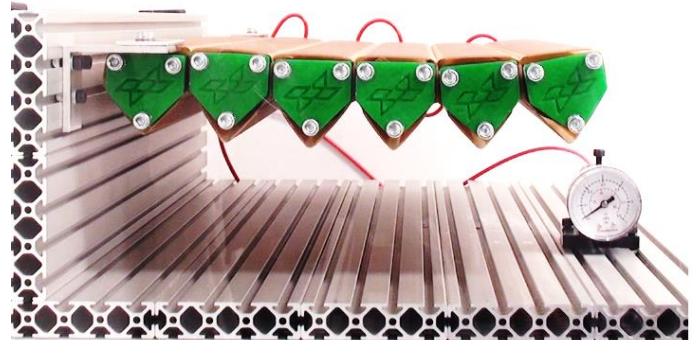


Figure 19: Demonstrator "Single Row Cantilever" at  $p=0\text{MPa}$ ,  $p_2=0.05\text{MPa}$  and  $p_3=0.15\text{MPa}$



necessary information for the cells adaptive characteristic, the deformation over pressure graph. Additionally the determination of material strains are enabled by strain gages, which are applied to the cell structure at the hinges  $k = 1, 2, 3$ . Figure 20 shows the demonstrator clamped within its test bed.



Figure 20: Demonstrator "Single Cell" within test bed

In contrast to the Single Cell Demonstrator, the Single Row Cantilever is built to show the potentials of the PACS concept. As the mechanical loading could be measured already with the single cell, this demonstrator is used to validate two important states. On the one hand the overall deformation at a maximum pressure of 0.2MPa is to be measured. Beyond that the functionality of the concept for crossing areas between neighbored cells should be proven. The maximum deformation of 123° could be measured at 0.2MPa at cell side  $j = 1$ . The process of deformation during pressurization can be seen in Figure 19.

## 6 Evaluation

For the verification of analytical and numerical results, the pressure dependent deformations and material stresses of the single cell are logged and compared with the calculated values. The single row cantilever is used to verify the deformation at the maximum pressure.

### 6.1 Single Cell Prototype

The implementation of a mature manufacturing process for the GFRP single cell of 50mm width, 450mm length and 15° of asymptotic deformation, together with the tube cartridge system for pressurization, provides the first real life unit of PACS. The basic working principle of the cell is proved for its characteristic property the distortion over pressure behavior. This value is measured and compared with the analytical and numerical characteristic as shown in Figure 21.

The results show the already stated deviation between analytical and numerical values. The data from the experimental investigations is rectified to consider the amount of pressure that is needed to inflate the elastomeric tube until it contacts the cell wall. The standard deviation for the experimental raw data is given. Except for the final descend of the measured graph the run of the three curves is similar. It shows a maximum variance against the numerical values of  $\eta_{exp.,FEM} = -22.40\%$ . The main reasons for this deviation lay in the geometrical deviations of the GFRP cell and the pressure distribution due to the Tube Cartridge system and are discussed in chapter 6.3.

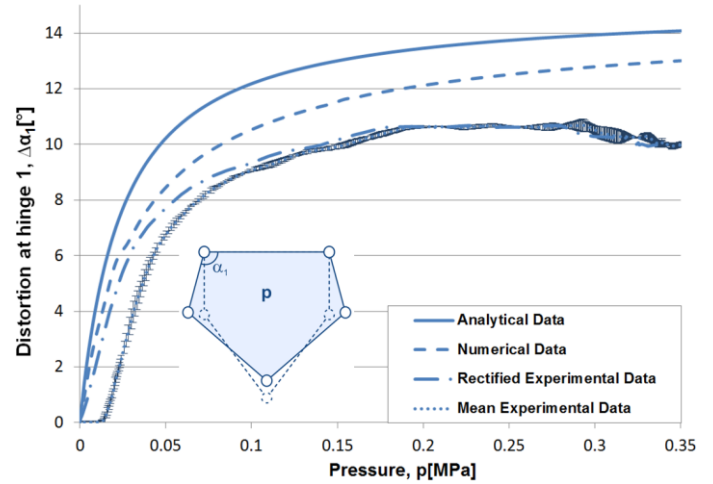


Figure 21: Comparison of analytical, numerical and experimental results for the angular distortion at hinge  $k=1$

The design concept optimizing cell wall and hinge geometries is verified by evaluating the strain gages. Figure 22 shows the maximum stress values in circumferential direction at the outer surface of the cell. The results from analytical and numerical calculations as well as from the processed strain gage data are plotted. The strain gages with a height of 0.6mm were applied centric to each hinge. Analogous to Figure 21 the raw mean experimental data is posted together with its standard deviation for hinge  $k = 1$ .

Besides the already seen deviations between computed and experimental results this figure shows a systematic source of divergence originated in improper model assumptions within the analytical approach. After an initial compliance the numerical and experimental values diverge from the analytical values. The underlying assumptions of infinite cell side stiffness and constant momentum distribution over hinge length are responsible for this behavior. Additional strain gages at the mid of face  $j = 1$  reinforce the suspicion that the deformation due to a pressure dependent negative bending moment at the cell sides leads to an additive charge of hinge  $k = 1, 3$  and a discharge of hinge  $k = 2$  (cp. Figure 11).

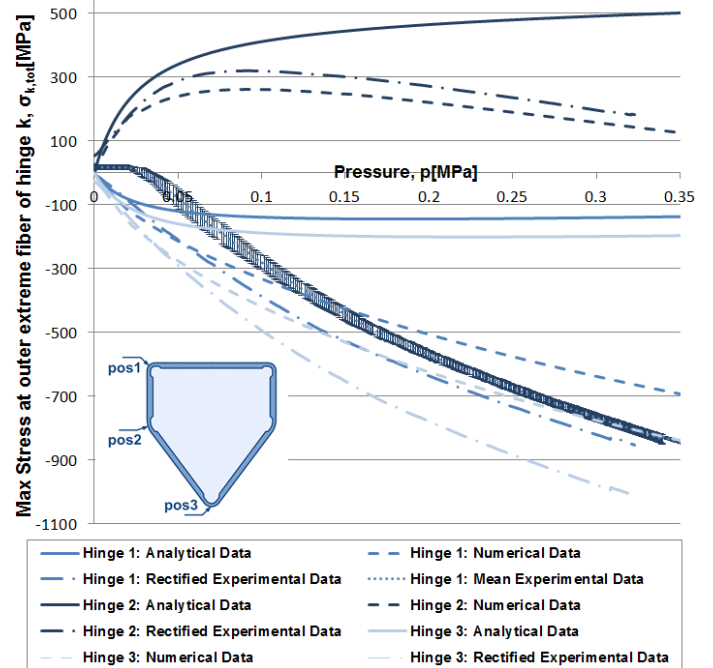
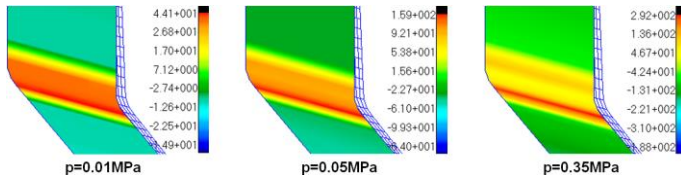


Figure 22: Max Stress values  $\sigma_{k,tot}$  over pressure  $p$  from analytical, numerical and experimental investigations at the outer surface of hinges  $k = 1, 2, 3$



The main reason for the wide variations between analytical and numerical respectively experimental results is based on the inconstant course of momentums. Figure 23 shows the stresses at hinge  $k = 2$  for increasing pressures. The maximum stresses move from a centric position and concentrate at the lower boundary of the hinge element. Both, the concentration of maximum stresses accompanied by huge stress gradients and their eccentric shift are responsible for the depicted graphs. Hinge elements with increased stiffness values and significantly risen maximum stresses result. At the hinge lines  $k = 1,3$  the maximum stress stay at the element's center during raise of pressure. For static and fatigue considerations these local stress concentrations dominate the limitations for the overall structural strength.



**Figure 23: Stress distribution [MPa] at outer surface of hinge  $k = 2$  in circumferential direction at different pressures  $p$**

Dropping the assumption of rigid cell sides and constant hinge momentums would produce remedy for the analytical approach. An optimization of these elements would further improve the structural performance and extend the design envelope of PACS.

## 6.2 Single Row Cantilever

A first insight into the potentials of PACS is given by the single row cantilever demonstrator. The experimental investigations of this structure summarize the results of the preliminary design process, the numerical verification, the manufacturing and the pressurization concept. Figure 19 shows the specimen for pressures of  $p = 0.0MPa$ ,  $0.05MPa$  and  $p_{max} = 0.2MPa$ . Note that the combination of gravitational force and hinge stiffness results in a slight initial deformation of the cantilevered beam.

For the sixth cell the surface related face  $j = 1$  performs an angular deflection of  $123^\circ$  at  $p = 0.2MPa$ . The comparison of numerical and experimental results leads to a deviation of  $\eta_{exp.,FEM} = +13.22\%$ , a reasonable result. This increased deformation of the experimental structure is due to reduced wall thickness at the hinge elements. An average value of  $t = 0.22mm$  instead of  $t = 0.25mm$  was measured ( $\sigma = 0.0141$ ) at the real test specimen. The adjusted hinge thickness leads to a deformation of  $\Delta\beta_{6,1,FEM} = 114.55^\circ$  and a deviation of  $\eta_{exp.,FEM} = 7.38\%$ .

**Table 7: Comparison of deformation results for the single row cantilever at cell side one of cell six at  $p = 0.2MPa$**

$\Delta\beta_{6,1,an} [^\circ]$	$\Delta\beta_{6,1,FEM} [^\circ]$	$\Delta\beta_{6,1,exp} [^\circ]$	$\eta_{exp.,FEM} [\%]$
134.54	108.64	123	+13.22

## 6.3 Discussion of results

The deviations between numerical and analytical respectively experimental values give reason for a discussion of errors. Each of the two data sources that are compared with the numerical values brings some error potential with it. The standard deviations in Figure 21 and Figure 22 show that the systematical failure exceeds random ones. Hence the underlying reasons are illuminated within this chapter. Analytical assumptions, manufacturing imperfections and deviants as well as experimental factors of influence can be differentiated.

The analytical equations are valid for the two-dimensional space and the underlying assumptions. Stresses due to lateral

contraction are thus not integrated. The resulting stresses are also underestimated by assuming constant momentums over the hinge lengths. As it was shown for the compliant hinges two and four, the stress gradient leads to stresses that overtop the analytically calculated distributed loads considerably. The finite stiffness of the cell side elements causes deformations which superimpose with the hinge distortions in the real life structure. The assumption of rigid cell sides does neglect this relation. Equally to the distribution of momentums the declaration of a single value for the hinge stiffness modelled as rotational springs reduces accuracy. The analytical model is in need of a one-dimensional hinge with a certain position. In reality a distributed hinge line exists which is inconstantly loaded with distortion what leads to a complex stiffness behavior that cannot be reproduced by the simple approach introduced in chapter 3.2. Effects of these mechanisms on the overall deformation are largely intercepted by the low rigidity of the hinge structure. Local stress values however are thereby strongly influenced as it can be obtained from Figure 23. The adapted cell geometry was only used for the cantilever demonstrator and does not influence the results for the single cell.

Manufacturing imprecisions build the second pool for error. Thickness variations at the hinge areas could be measured and lay at about -12%. This amount of wall thickness reduction influences the equilibrium state of the structure and increases the overall deformation through a reduction of stiffness. The variance of face thicknesses is also measured and stated between 0% and -3.2%. The draping accuracy of a hand-made GFRP component as well as differing material constants are further possible sources of error that could not be eliminated but have minor impact. Thermal expansion of the silicone core during the GFRP processing could most widely been neglected by simulation.

Factors of influence related to the experimental setup are revealed at the positioning of strain gages (see chapter 6.1). Experimental and numerical values can only be compared for exactly positioned strain gages and moderate strain gradients compared to the measurement influencing area. The mechanical behavior of the coupled system of pressure tube and cellular structure leads to a non-constant pressure distribution and also corresponds to the experimental setup.

Primarily material stresses could not be calculated in a satisfying way with the analytical methods. Concepts for avoiding the responsible sources of error are found and will be integrated in the design process of PACS in further works.

## 6.4 Prospect: Double Row Cantilever

The stiffening phase can only be reached in a single shape state with a single row PACS. A second row is necessary to complete the functionality of this morphing concept and thus is examined in a further step. A double row cantilever is built from the isotropic material Polyamid12 with a Young's modulus of 1300MPa and consists of eight plus two pentagonal and seven hexagonal cells. Figure 24 shows the analytical and numerical deformation results as well as the appropriate material stresses. A mature design process allows to adjust these values to fulfill also service life requirements.

Since this geometry of the structure is not bound by the manufacturing requirements of laminated FRP, compliant hinges and face regions can be shaped in a more valuable way. In order to extend the verification of the concept of PACS, the implementation of this double row cantilever shall provide the necessary data. Therefore, the analytical model is upgraded for the purpose of covering multiple rows. A geometrical design

with the dimensions 450x400x85mm is processed and the first numerical simulations are performed on the basis of the analytical outcomes.

A deviation of 4.14% of angular cell side distortion at the upper boundary ( $j = 1$ ) of the eighth cell against the numerical values confirms the analytical approach. In the subsequent work it will be refined to drop assumptions and thereby enhance the results. The double row cantilever has been manufactured and will be used for physical examinations in the ongoing work.

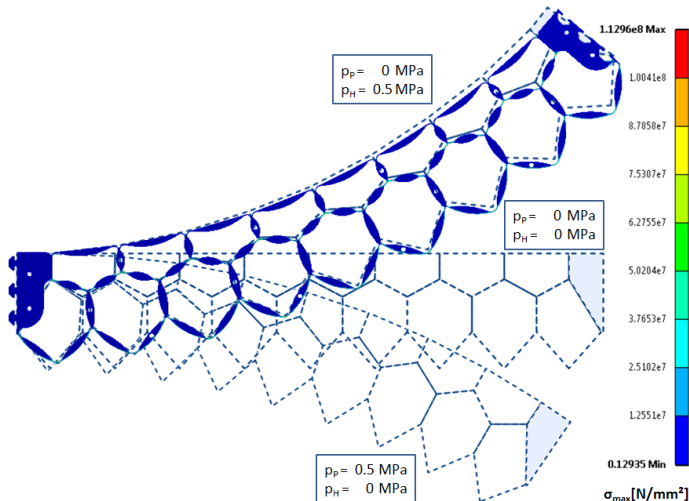


**Figure 24: Double Row Cantilever - Analytical and numerical results for deformation at  $p=0.5\text{MPa}$ ; von Mises stress results for numerical simulation**

## 7 Conclusion

The most important demand on each shape variable structure is defined by the imperative need for advance. With the concept of pressure actuated cellular structures an energetically efficient idea with lightweight potentials is investigated, which combines structure and actuator in a single component.

A single cell and a single row cantilever demonstrator with the dimensions  $450 \times 300 \times 50\text{mm}^3$  was built and investigated experimentally under pressure load. For the given geometrical boundary conditions FRP showed to be the most efficient material for the PACS test specimens. It is shown analytically how the geometrical design of the hinge elements significantly influences the cells' pressure dependent deformation characteristic and stiffening performance.

The manufacturing of the PACS structures in a prepreg process holds challenges especially for the sensitive hinge regions. Wrinkles could be prevented by an adaption of the autoclave process by utilizing thermal expansion of the mold core. As functional part of the structure, geometrical accuracy is critical in this area and has to be handled carefully.

A pressurization system was implemented which can withstand pressures up to  $0.35\text{MPa}$ , but still defines the load limit for the PACS structure.

With the GFRP material Hexply 913 and a minimum wall thickness of  $0.2\text{mm}$  a total deflection of  $123^\circ$ ,  $12.3^\circ$  per cell side, was reached with the single row cantilever demonstrator at  $p = 0.2\text{MPa}$ . A deviation of  $13.22\%$  between experimental and numerical cell side deformations was measured. The evaluation of analytical and numerical with experimental data shows principled accordance. Major differences in stress distributions reveal the necessity for extending the analytical approach. A test for validity of the fundamental design strategy was performed and the effects of assumptions were discussed.

Research on the mechanical properties of eccentric compliant hinges with reference to the PACS will enhance the analytical approach. Together with the consideration of conceptual or manufacturing-based thickness limitations and fatigue treatment this will result in an updated design envelope. Adapted to a double row cantilever structure these results are going to generate a better insight in the potential of the concept. Overcoming these steps will allow examining a given PACS for mechanical properties, for deformation efficiency or aerodynamic behavior.

## 8 Literature

- Ajaj R.M. et al. (2012, December). The Zigzag wingbox for a span morphing wing. *Aerospace Science and Technology*, pp. 364-375.
- Barrett R. et al. (1996, April). Missile flight control using active. *Smart Materials and Structures*, pp. 121-128.
- Barrett R. et al. (2010). *Patent No. EP 2459442 A2*. Europe.
- Barrett R. et al. (2014, June). Biomimetic FAA-certifiable, artificial muscle structures for commercial aircraft wings. *Smart Materials and Structures*.
- Bauer, C. (2000). *Die Rippenlose Wölbklappe - Realisierung eines formvariablen Tragflügelprofils zur aerodynamischen Leistungsoptimierung zukünftiger Verkehrsflugzeuge*. Aachen: Shaker Verlag.
- Böge, A. (2007). *Formeln und Tabellen Maschinenbau*. Wiesbaden: Friedr. Vieweg & Sohn Verlag.
- Elzey D. et al. (2003). A bio-inspired, high-authority actuator for shape morphing structures. *Smart Structures and Materials*, pp. 92-100.
- Hornbogen, E. (2006). *Werkstoffe*. Berlin: Springer-Verlag.
- Howard, R. (1991, December). Penetration of hard substrates by a fungus employing enormous turgor pressures. *Proceedings of the National Academy of Sciences of the United States*, pp. 11281-11284.
- Huber J. E. et al. (1997, October). The selection of mechanical actuators. *The Royal Society*, pp. 2185-2205.
- Janocha, H. (1992). *Aktoren - Grundlagen und Anwendungen*. Berlin: Springer Verlag.
- Kern, G. (2014, Juni 2). *Kern, Technische Kunststoffteile und Halbzeuge*. Retrieved Juni 2, 2014, from Kern.de: <http://www.kern.de/>
- Luo Q. et al. (2013, April). Adaptive pressure-controlled cellular structures for shape morphing: II. Numerical and experimental validation. *Smart Materials and Structures*, pp. 1-12.
- Monner, H. P. (2001, December). Realization of an optimized wing camber by using formvariable flap structures. *Aerospace Science and Technology*, pp. 445-455.
- Mueller, D. (2000). *Das Hornkonzept - Realisierung eines formvariablen Tragflügelprofils*. Frankfurt.
- Pagitz M. et al. (2011). *Patent No. Patent 2006936*. Netherlands.
- Pagitz M. et al. (2012, January). Pressure-actuated cellular structures. pp. 1-19.
- Pagitz M. et al. (2014). Compliant Pressure Actuated Cellular Structures. arXiv 1403.2197.
- Ramrakhiani D. et al. (2005, November/December). Aircraft Structural Morphing Using Tendon-Actuated. *Journal of Aircraft*, pp. 1615-1621.
- Sibaoka, T. (1991, January). Rapid plant movements triggered by action potentials. *The Botanical Magazine*, pp. 73-95.
- Sun Z. et al. (2003, April 15). Modeling of fatigue damage in a polymer matrix composite. *Materials Science & Engineering*, pp. 302-311.

- Vasista S. et al. (2013, August). Topology-optimized design and testing of a pressure-driven morphing-aerofoil trailing-edge structure. *AIAA Journal*, pp. 1898-1907.
- Vos R. et al. (2010, April). Pressure Adaptive Honeycomb: Mechanics, Modeling, and Experimental Investigation. *AIAA*, pp. 2010-2023.
- Vos R. et al. (2010). *Patent No. US Pat 8366057*. USA.
- Wacker, C. A. (2014, Juni 2). *Wacker.com*. Retrieved Juni 2, 2014, from Fest- und Flüssigsiliconkautschuk: [http://www.wacker.com/cms/media/publications/downloads/6709\\_DE.pdf](http://www.wacker.com/cms/media/publications/downloads/6709_DE.pdf)
- Weißbach W. (2007). *Werkstoffkunde, Strukturen, Eigenschaften, Prüfung*. Wiesbaden: GWV.